

TEST PARTICLE ENERGIZATION AND THE ANISOTROPIC EFFECTS OF DYNAMICAL MHD TURBULENCE

C.A. GONZÁLEZ,¹ P. DMITRUK,¹ P.D. MININNI,¹ AND W.H. MATTHAEUS²

¹*Departamento de Física, Facultad de Ciencias Exactas y Naturales, Universidad de Buenos Aires and IFIBA, CONICET, Ciudad universitaria, 1428 Buenos Aires, Argentina*

²*Bartol Research Institute and Department of Physics and Astronomy, University of Delaware, Newark, Delaware, USA*

Submitted to ApJ

ABSTRACT

In this paper we analyze the effect of dynamical three-dimensional MHD turbulence on test particle acceleration, and compare how this evolving system affects particle energization by current sheets interaction, against frozen-in-time fields. To do this we analyze the ensemble particle acceleration for static electromagnetic fields extracted from direct numerical simulations of the MHD equations, and compare with the dynamical fields. We show that a reduction in particle acceleration in the dynamical model results from the particle trapping in the field lines, which forces the particles to remain in a moving current sheet that suppress the longer exposure at the strong electric field gradients located between structures, which is an efficient particle acceleration mechanism. In addition, we analyze the effect of anisotropy caused by the mean magnetic field. It is well known that for sufficiently strong external fields, the system suffers a transition towards a two-dimensional flow. This causes an increment in the size of the coherent structures, resulting in a magnetized state of the particles and the reduction of the particle energization.

Keywords: Particle acceleration, MHD Turbulence, Coherent structures, Magnetized plasmas

1. INTRODUCTION:

The production of energetic particles in the Earth-Sun environment and in the interstellar medium brings the open question of what are the mechanisms behind the generation of their non-thermal charged particle population (Parker and Tidman (1958)). In all these systems the flows are turbulent, as the turbulent plasma state is observed in almost all astrophysical and space physics systems. Acceleration of charged particles by turbulence in the solar corona is also one of the candidates to explain coronal heating, as well as the origin of solar wind energetic particles observed at *in-situ* measurements and at ground-based observatories (McComas et al. (2007)).

As a result, many authors have studied and reported charged particle acceleration by plasma turbulence (Matthaeus et al. (1984); Lazarian et al. (2012)). In general, in these problems turbulence covers a huge range of spatio-temporal scales, from low frequency events well described by fluid plasma models (such as magnetohydrodynamics or MHD, or Hall-MHD), up to very high-frequency scales related to electron dynamics which are well described by purely kinetic approaches.

In order to capture at least a fraction of the range of scales involved in plasma turbulence, test particle simulations in MHD flows have been used as a way to understand how the macroscopic behavior of a plasma could itself generate plasma heating and particle energization. This problem has been treated in different ways, which can be divided into two broad approaches. The first one consists on modeling the turbulence as a random collection of waves (Chandran (2003); Chandran and Maron (2004); Cho and Lazarian (2006); Lynn et al. (2013)), a representation that cannot retain the coherent structures formation and evolution, and which in particular can play a crucial role in particle energization (Matthaeus et al. (1984); Tessein et al. (2015)). In the second approach, the turbulence is generated as a result of the normal evolution of the MHD fluid equations (Dmitruk et al. (2004); Dmitruk and Matthaeus (2006); Lehe et al. (2009); Teaca et al. (2014); Dalena et al. (2014); Weidl et al. (2015)), and as such it self-consistently includes the evolution of coherent structures. However, test particle studies have been mostly carried out using static fields obtained from the direct numerical simulation of the MHD equations (i.e., the system is evolved in time to reach a turbulent regime, and then a frozen-in-time snapshot of electric and magnetic fields is used to compute particle acceleration). The problem with this method is that it ignores the evolution of the coherent structures, and that it does not allow for the presence of waves.

Although there are some works that deal with the influence of dynamic MHD turbulence on test particles (Lehe et al. (2009); Teaca et al. (2014)), those papers does not make a complete analysis of the dynamical fields effect which is in principle our goal in this paper. Besides, the comparison between static and dynamic cases allow us to determine what is the most relevant mechanism for particle heating between particle-wave resonance or the interaction with well developed coherent structures in the turbulent flow.

Then, the first aim of this paper is therefore to look at the effect of dynamical turbulence evolution on particle energization. To this end, we performed different direct numerical simulations of MHD turbulence, together with solving the equations for test particles with a gyroradius of the order of the MHD dissipation scale, first in static and then in dynamic electromagnetic fields, and for different values of a mean external magnetic field B_0 .

We found a reduction of particle energization in the dynamical case, and that this reduction is the result of particle trapping into the dynamic current sheets. This trapping reduces the exposure time in the strong electric field gradient regions at the interface between current sheets, that is essentially needed for particle energization. In spite of this reduction, the results validate previously reported particle acceleration mechanisms in MHD turbulence (Matthaeus et al. (1984); Dmitruk et al. (2004); Teaca et al. (2014); Dalena et al. (2014); Gonzalez et al. (2016)), and it shows the importance of coherent structures in particle acceleration phenomena.

The second aim of this paper is also to quantify the role of the mean external field B_0 in coherent structure formation and particle acceleration, as in many cases in space physics particle acceleration takes place in the presence of a guide field. To do this, we performed a set of simulations varying from an isotropic case ($B_0 = 0$) up to a strong anisotropic case with a mean field $B_0 = 8$ (in units of the fluctuating magnetic field \mathbf{b}). We show that the anisotropy induced by the mean magnetic field produces large coherent structures as the mean field increases. Consequently, for large magnetic field the particles remain magnetized, that is, attached closely to magnetic field lines, and then cannot transport across the current sheets, decreasing the possibility to stay long time in regions where the electric field gradient is strong, between current structures. The particle propagation along the magnetic field lines then suppress the acceleration due to perpendicular electric field gradients between current sheet structures.

The organization of this paper is as follows: In section 2 we describe the model used in our investigations, the

equations and properties of turbulent MHD fields, and the test particle model including the parameters that relate particles and fields. In section 3.A we present a comparison between the static and dynamical cases for an isotropic case with $B_0 = 0$ and for an anisotropic case with $B_0 = 2$. In section 3.B we discuss the effect of the mean magnetic field on coherent structures and particle acceleration. Finally, in section 4 we discuss our findings and present our conclusions.

2. MODELS:

The macroscopic description of the plasma adopted here is modeled by the three-dimensional compressible MHD equations: the continuity (density) equation, the equation of motion, the magnetic field induction equation, and the equation of state. These are given respectively by Equations. (1-4), which involve fluctuations of the velocity field \mathbf{u} , magnetic field \mathbf{b} , and density ρ . We assume a large-scale background magnetic field B_0 in the z -direction, so that the total magnetic field is $\mathbf{B} = \mathbf{B}_0 + \mathbf{b}$ with $\mathbf{B}_0 = B_0 \hat{z}$,

$$\frac{\partial \rho}{\partial t} + \nabla \cdot (\mathbf{u} \rho) = 0, \quad (1)$$

$$\frac{d\mathbf{u}}{dt} = -\frac{\nabla p}{\rho} + \frac{\mathbf{J} \times \mathbf{B}}{4\pi\rho} + \nu \left(\nabla^2 \mathbf{u} + \frac{\nabla \nabla \cdot \mathbf{u}}{3} \right) + \mathbf{F}, \quad (2)$$

$$\frac{\partial \mathbf{B}}{\partial t} = \nabla \times (\mathbf{u} \times \mathbf{B}) + \eta \nabla^2 \mathbf{B} + \nabla \times \boldsymbol{\varepsilon}, \quad (3)$$

$$\frac{p}{\rho^\gamma} = \text{constant}. \quad (4)$$

Here p is the pressure, ν the viscosity, η the magnetic diffusivity, $\mathbf{J} = \nabla \times \mathbf{B}$ is the current density, \mathbf{F} is an external mechanical force, and $\boldsymbol{\varepsilon}$ is an external electromotive force. We assume a polytropic equation of state $p/p_0 = (\rho/\rho_0)^\gamma$, with $\gamma = 5/3$, where p_0 and ρ_0 are respectively the equilibrium (reference) pressure and density. The Hall current is not taken into account in equation.(3) but will be (nominally) later included on the particle motion equations through the generalized Ohm's law for the electric field. The reason for that is that the dynamics of the \mathbf{u}, \mathbf{B} fields described by equations (1)-(4) is not importantly affected by the presence of the Hall term, provided that the Hall scale (see below) is close to the dissipation scale (see [Dmitruk and Matthaeus \(2006\)](#)).

The magnetic and velocity fields here are expressed in Alfvén speed units based on field fluctuations. This Alfvén speed based on field fluctuations is defined as $v_0 = \sqrt{\langle b^2 \rangle} / 4\pi\rho_0$. A characteristic plasma velocity can

also be given by the parallel Alfvén wave velocity along the mean magnetic field $v_A = B_0 / \sqrt{4\pi\rho_0}$; this is proportional to the amplitude of guide field. The ratio of fluid equilibrium pressure p_0 to magnetic pressure B_0^2 , the so-called β of the plasma, is $\beta = p_0/B_0^2 = 1/(MB_0)^2$. The sonic Mach number $M = v_0/C_s$ relates the mean velocity field with the sound speed $C_s = \sqrt{\gamma p_0/\rho_0}$. We use the isotropic MHD turbulence correlation length L as a characteristic length (also called the energy containing scale), defined as $L = L_{box} \int (E(k)/k) dk / \int E(k) dk$, where $E(k)$ is the energy spectral density at wavenumber k , and L_{box} is the linear size of the domain. The unit timescale t_0 , also called the eddy turnover time, is derived from the unit length and from the fluctuation Alfvén speed $t_0 = L/v_0$.

The MHD equations are solved numerically using a Fourier pseudospectral method with periodic boundary conditions in a normalized cube of size $L_{box} = 2\pi$; this scheme ensures exact energy conservation for the continuous-time spatially-discrete equations in the ideal ($\nu = \eta = 0$) and not forced ($\mathbf{F} = \boldsymbol{\varepsilon} = 0$) case ([Mininni et al. \(2011\)](#)). The discrete time integration is done with a high-order Runge-Kutta method, and a resolution of 256^3 Fourier modes is used. For the kinematic Reynolds number $R = v_0 L / \nu$ and the magnetic Reynolds number $R_m = v_0 L / \eta$, we take $R = R_m = 1000$, which are limited here by the available spatial resolution. The Mach number in our simulations is $M = 0.25$, so we consider a weak compressible case.

In [Gonzalez et al. \(2016\)](#). We reported the effect of the compressibility of the flow on particle acceleration. In that study we considered decaying turbulence from an initial perturbation, and after the turbulence was fully developed, the test particles were injected into the system and evolved in a frozen-in-time snapshot of the turbulent electromagnetic field. As in this paper we are interested in studying the effect of dynamically evolving turbulence, to maintain energy fluctuating around a mean value (i.e., to reach a turbulent steady state) we must force the system externally using the mechanical and electromotive forces \mathbf{F} and $\boldsymbol{\varepsilon}$ in Equations. (2) and (3).

To this end we started the system from initially null magnetic and velocity fields and forced until to get a quasi-stationary MHD state. The forcing scheme that we employed (for both \mathbf{F} and $\boldsymbol{\varepsilon}$) in all the simulations showed here is based on that presented in [Pouquet and Patterson \(1978\)](#). The forcing introduces (on the average) zero mechanical and magnetic helicity, and zero cross-correlation between the velocity and magnetic field fluctuations. We used slowly-evolving random-phases forcings in the Fourier k -shells with $3 \leq k \leq 4$, with a

correlation time $\tau = t_0$. In other words, in each eddy turnover time new random (and uncorrelated) forcing functions \mathbf{F} and $\boldsymbol{\varepsilon}$ were generated, and each forcing was linearly interpolated in time from the previous random state to the new one in a time t_0 . In this way we prevented introducing sudden changes in the field that may arise when delta-correlated in time forcing is used, and which may affect the evolution of test particles.

Each random snapshot of the forcing functions was generated as follows. For a forcing \mathbf{f} (which may be either \mathbf{F} or $\boldsymbol{\varepsilon}$), we generated first two random fields in Fourier space,

$$\mathbf{v}_j^{(1)}(\mathbf{k}) = A(k)e^{i\phi_j}, \quad \mathbf{v}_j^{(2)}(\mathbf{k}) = A(k)e^{i\psi_j}, \quad (5)$$

where $j = 1, 2, 3$ are the field Cartesian components, $\phi_j(\mathbf{k})$ and $\psi_j(\mathbf{k})$ are random phases, and $A(k)$ is 1 if $3 \leq k \leq 4$, and 0 otherwise. Two normalized incompressible fields are then constructed as

$$\mathbf{f}^{(1)} = \frac{\nabla \times \mathbf{v}^{(1)}}{\langle |\nabla \times \mathbf{v}^{(1)}|^2 \rangle^{1/2}}, \quad \mathbf{f}^{(2)} = \frac{\nabla \times \mathbf{v}^{(2)}}{\langle |\nabla \times \mathbf{v}^{(2)}|^2 \rangle^{1/2}}. \quad (6)$$

We introduce a correlation between these fields making use of the auxiliary quantity as

$$\omega_f = \nabla \times [\sin(\alpha)\mathbf{f}^{(1)} + \cos(\alpha)\mathbf{f}^{(2)}] \quad (7)$$

where α can take any value between 0 and $\pi/4$. Finally, the forcing function \mathbf{f} is given by

$$\mathbf{f}(\mathbf{k}) = f_0 \left[\cos(\alpha)\mathbf{f}^{(1)}(\mathbf{k}) + \sin(\alpha)\mathbf{f}^{(2)}(\mathbf{k}) + \frac{\omega_f(\mathbf{k})}{k} \right], \quad (8)$$

with f_0 the forcing amplitude. Note that α controls how much correlated is \mathbf{f} with its curl (in fact, this correlation is proportional to $\sin 2\alpha$). Thus, using $\alpha = 0$ gives a random forcing function that does not inject helicity on the average. This allows us to study cases in which there is no inverse cascade (as the presence of helicity in the three-dimensional flow can result in the growth of large scale structures as a result of the inverse cascade of magnetic helicity [Mininni \(2011\)](#)), which will be important to understand the role of the growth of correlation lengths as the flow becomes two-dimensional in particle acceleration for large values of B_0 .

When a stationary turbulent state was reached and a broad range of scales were excited, the test particles were injected and then both field and particles were simultaneously evolved (for frozen-in-time simulations, one snapshot of the fields was extracted, and only test particles were evolved). In the turbulent regime the fluid contains energy from the outer scale L to the Kolmogorov

dissipation scale $l_d = (\nu^3/\epsilon_d)^{1/4}$, where ϵ_d is the average rate of energy dissipation; then we can define the Kolmogorov dissipation wavenumber as $k_d = 2\pi/l_d$.

We must now introduce the equations for the test particles, and associate the particle parameters with the relevant flow parameters.

Test particle dynamics is described by the nonrelativistic equation of motion:

$$\frac{d\mathbf{v}}{dt} = \alpha(\mathbf{E} + \mathbf{v} \times \mathbf{B}), \quad \frac{d\mathbf{r}}{dt} = \mathbf{v}. \quad (9)$$

The electric field \mathbf{E} can be obtained from the generalized Ohm's law which can be dimensional scaling by $E_0 = v_0 B_0 / c$ as follows:

$$\mathbf{E} = -\mathbf{u} \times \mathbf{B} + \frac{\epsilon}{\rho} \mathbf{J} \times \mathbf{B} - \epsilon \nabla p_e + \frac{\mathbf{J}}{R_m}. \quad (10)$$

The dimensionless parameter α relates particles and MHD field parameters:

$$\alpha = Z \frac{m_p}{m} \frac{L}{\rho_{ii}}, \quad (11)$$

where ρ_{ii} is the proton inertial length given by $\rho_{ii} = m_p c / (e \sqrt{4\pi \rho_0})$, m is the mass of the particle, m_p is the mass of the proton, and Z is the atomic number (we will consider $m = m_p$ and $Z = 1$). The inverse $1/\alpha$ represents the nominal gyroradius, in units of L and with velocity v_0 , and measures the range of scales involved in the system (from the outer scale of turbulence to the particle gyroradius). One could expect a value $\alpha > 10^4$ specially for space physics and astrophysical plasmas, which represent a huge computational challenge due to numerical limitations.

Once the turbulent state was reached, 10000 test particles were randomly distributed in the computational box and the equation of motion for particles and the MHD electromagnetic fields were evolved. Equation (9) for each particle was evolved in time using a fourth-order Runge-Kutta method, and cubic splines were used to extrapolate the values of the terms in Eq. (10) from the three-dimensional MHD grid to the position of the particles. Particles were initialized with a Gaussian velocity distribution function, with a root mean square (r.m.s.) value of the order of the Alfvén velocity. It is well known that the particle gyroradius has a significant influence on the particle acceleration mechanisms, and our aim in this paper is to explore the dynamical effect of MHD turbulence on acceleration of large gyroradius particles, of the order of the turbulent dissipation length. Thus, we set $\rho_{ii} = l_d$. We will loosely call these particles “protons” as their gyroradius is at the end of the inertial range of our MHD simulations ([Dmitruk et al. \(2004\)](#)).

Table 1. Parameters of the simulations discussed in Sec. III.A. B_0 is the amplitude of the guide field, M is the sonic Mach number, β is the plasma “beta,” $\langle L \rangle$ is the average energy containing scale for the flow during the steady-state period, $\langle k_d \rangle$ is the average Kolmogorov dissipation wavenumber, and α is the nominal particle gyroradius.

Run	B_0	M	β	$\langle L \rangle$	$\langle k_d \rangle$	α
1	0	0.25	6.12	2.31	92	40
2	2	0.25	2.79	1.76	96	52.63

The second and the third terms in Eq. (10) are the Hall effect and the electron pressure gradient respectively. The dimensionless coefficient ϵ is the Hall parameter:

$$\epsilon = \frac{\rho_{ii}}{L} \quad (12)$$

Those two terms in Eq. (10) are important at small scales, especially at the proton gyroradius but they make small contributions to the fluid equations through the curl of \mathbf{E} (i.e. single-fluid compressible MHD is still appropriate at large scales). However one must expect them to impact the acceleration of particles by their contribution to the electric field \mathbf{E} (Kulsrud. (1983)).

The Hall parameter relates the ion inertial length scale with the energy containing scale. Thus, for consistency with the test particle definition (see Eq. 11), we set the value of the Hall parameter $\epsilon = 1/\alpha$ in our simulations. In the MHD description it is assumed that plasma protons and electrons are in thermal equilibrium, i.e., their pressures are $p_e = p_i$. Then $p_e = p/2$ with $p = p_e + p_i$ the total pressure. For particles with $\alpha = 1/\epsilon$ and $\rho_{ii} = l_d$ (as is the case studied here), we showed in Gonzalez et al. (2016) that the second and third terms on the r.h.s. of equation. (10) give a negligible contribution to the acceleration. We will however preserve these terms for consistency. The case of small particle gyroradii (such as particle with a real mass electrons), which was also previously reported, those terms become really relevant, and we will left for a future study about the effect of dynamical electromagnetic fields over that kind of particles.

3. RESULTS:

3.1. Dynamic vs. static MHD fields

In this section we compare the particle behavior for static and dynamic MHD fields, in two different scenarios with and without an external mean magnetic field. Table 1. presents the parameters of the flow and of the particles for the simulations in this section.

In Figure. 1 we show the kinetic and magnetic energy for the time-evolving simulations with $B_0 = 0$ and

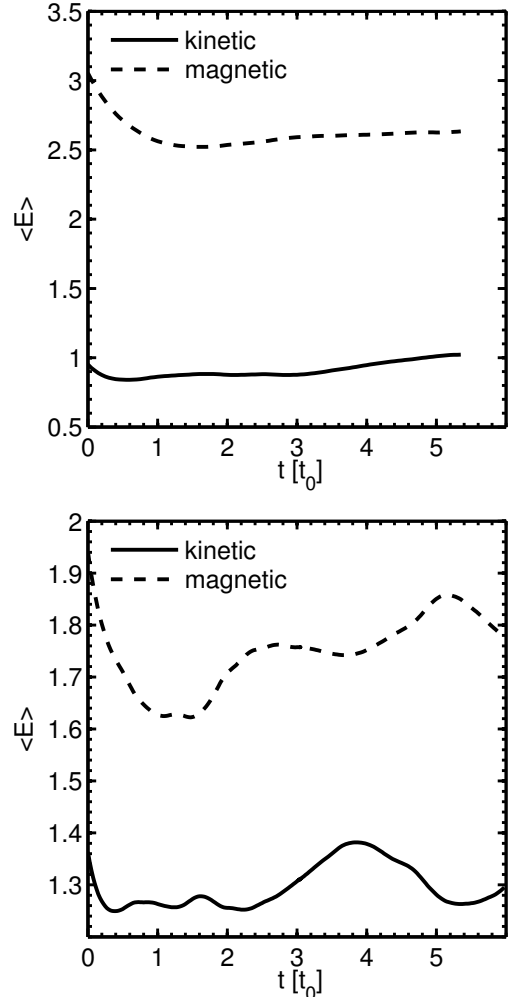


Figure 1. Mean energy of MHD variables as function of time, (*top*) for a simulation with no mean magnetic field mean field simulation ($B_0 = 0$) and (*Bottom*) for simulation with $B_0 = 2$.

$B_0 = 2$ during the time that particles are running simultaneously with the fields. The MHD fields are initially started from a null initial state and then a forcing is applied from the beginning of the simulation to obtain a quasi-stationary state (at about $\sim 15t_0$). Note that the system is in a turbulent steady state, with the energy fluctuating around a mean value. As a reference, once the particles are added to this flow, it takes about 5 turnover times for the particles to cross the entire simulation box (periodic boundary conditions are used for both the fluid and the particles, and thus the most energetic particles can re-enter the box and travel larger distances).

The mean square displacement D_r as a function of time is shown in Figure. 2, for the simulations with $B_0 = 0$ and with $B_0 = 2$, for both the static and dy-

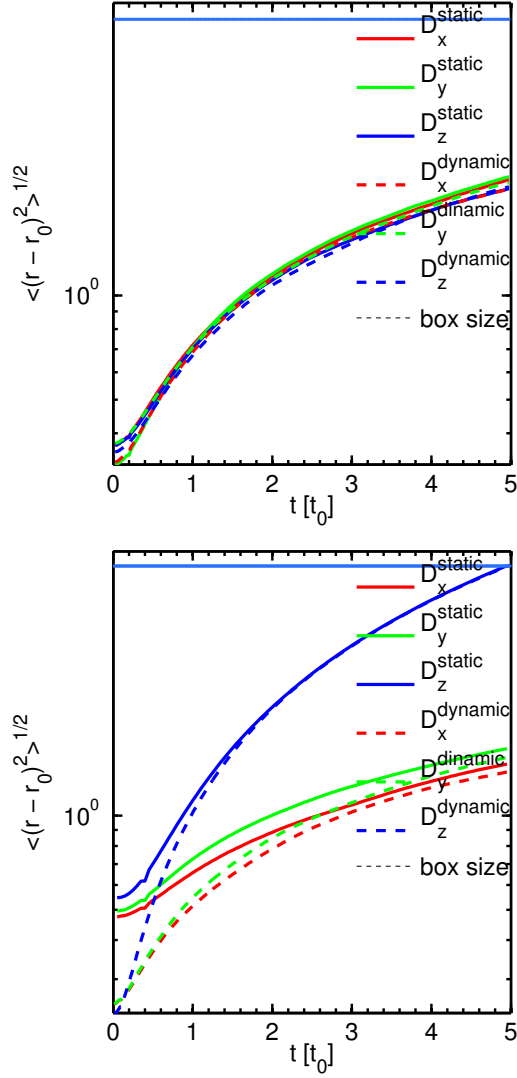


Figure 2. Mean square displacement of protons as function of time in box units, for the static (solid line) and dynamic (dashed line) simulations. (*Top*) Simulation without mean magnetic field ($B_0 = 0$), and (*Bottom*) simulation with a mean magnetic field $B_0 = 2$. The dashed line indicates the size of the simulation box.

dynamic cases. Again by “static case,” we refer to the case in which a snapshot of the fields is frozen in time, and the particles are evolved in the electric and magnetic fields (as done in previous studies, see e.g., Refs. [Dmitruk et al. \(2004\)](#); [Dmitruk and Matthaeus \(2006\)](#); [Dalena et al. \(2014\)](#)). In the “dynamic case” the equations of motion of the particles are evolved in time together with the MHD equations, and thus the particles are affected by the time evolution of the structures in the flow. A small difference is observed between these two cases, with a slightly larger mean displacement in the static case. Additionally, the displacement of the test particles in the

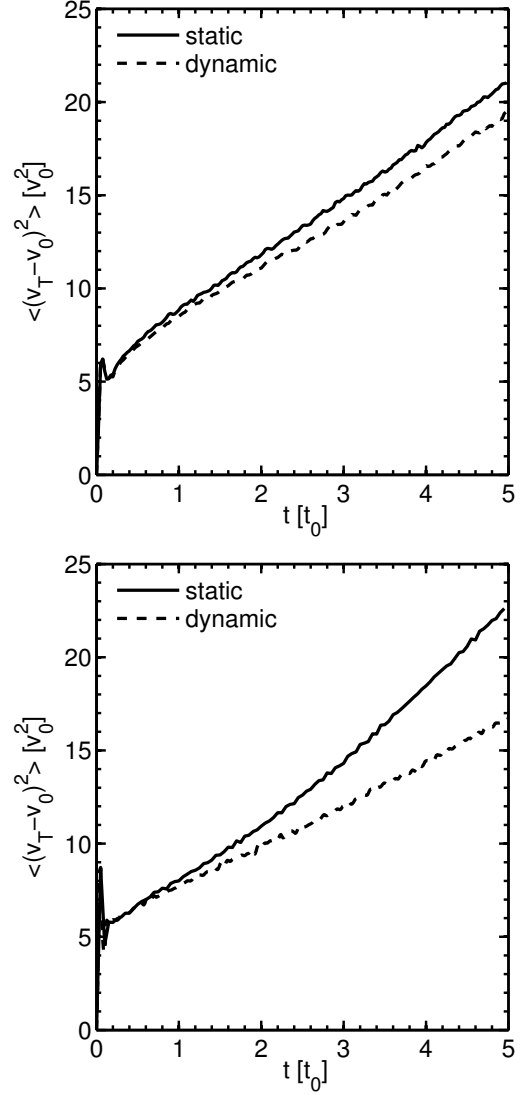


Figure 3. Mean square velocity of protons as function of time for the static (solid line) and dynamic (dashed line) cases. (*Top*) Simulation without mean magnetic field ($B_0 = 0$) and (*Bottom*) with mean magnetic field ($B_0 = 2$).

z direction in the simulation with $B_0 = 2$ changes significantly (when compared with the case with $B_0 = 0$), as a result of the test particles following the direction of the mean magnetic field. While in the run with $B_0 = 0$ the dispersion is isotropic (i.e., the mean displacement is the same within statistical errors for the x , y , and z directions), in the run with $B_0 = 2$ much larger displacements are observed in the z direction.

In Figure. 3 we show the mean square velocity as function of time, $v_T^2 = v_\perp^2 + v_\parallel^2$, i.e., the sum of the squared parallel and perpendicular components of the test particle velocities, averaged over all test particles. Results for the isotropic and the anisotropic cases are shown,

comparing also the static and dynamic cases. A smaller mean velocity at late times is observed in the dynamic case, specially for the case with $B_0 = 2$.

The progressive increment in the mean square velocity is the result of the interaction with the electric fields near the current sheets found along the particle trajectory, as was described in a previous paper [Gonzalez et al. \(2016\)](#). In the isotropic case, the structures are randomly distributed in the box and there is no privileged direction; as a result the current sheets are not aligned and are instead randomly oriented. This situation and the lack of a large magnetic field make the particles interact with several different structures along its path and to be exposed to the strong gradient electric field regions for long times. The reduced final r.m.s velocity in the dynamic case, instead, is associated with the dynamic coherent structures that trap particles and reduces this exposure time that is an essential component for particle acceleration.

In Figure. 4 we show the probability density function (PDF) of particle energy for the isotropic and anisotropic cases (and for both the static and dynamic cases). In the isotropic case, the distributions for static and dynamic fields are very similar. There is only a slightly larger value of probability in the core of the distribution (i.e., for low squared velocities) in the dynamic case, which can be understood as we already noted that in the dynamic case the acceleration of particles is slightly less efficient. However, in the anisotropic case these differences become somewhat larger (although still small in absolute terms), accompanied with a shorter tail in the PDF for the dynamic case at large squared velocities. In the presence of the the mean field more particles are accelerated, and with larger energies, in the static case than in the dynamic case.

As discussed above, visual exploration of the particles trajectories indicate that the fact that particles are more accelerated in the static case than in the dynamic case is the result of particles being able to interact for longer times with multiple current sheets (i.e., they can move from one current sheet to another, and cross strong electric fields gradients in their paths), and thus can obtain larger energies. Meanwhile, in the dynamic case the particles are trapped for longer times in an individual current sheet advected by the flow, and cannot easily move in the strong gradient regions, which is the most efficient process to accelerate them.

With this in mind, in the next section we explore the effect of the mean magnetic field on particle acceleration in the dynamically evolving turbulent electromagnetic field. To this end, we analyze particle energization vary-

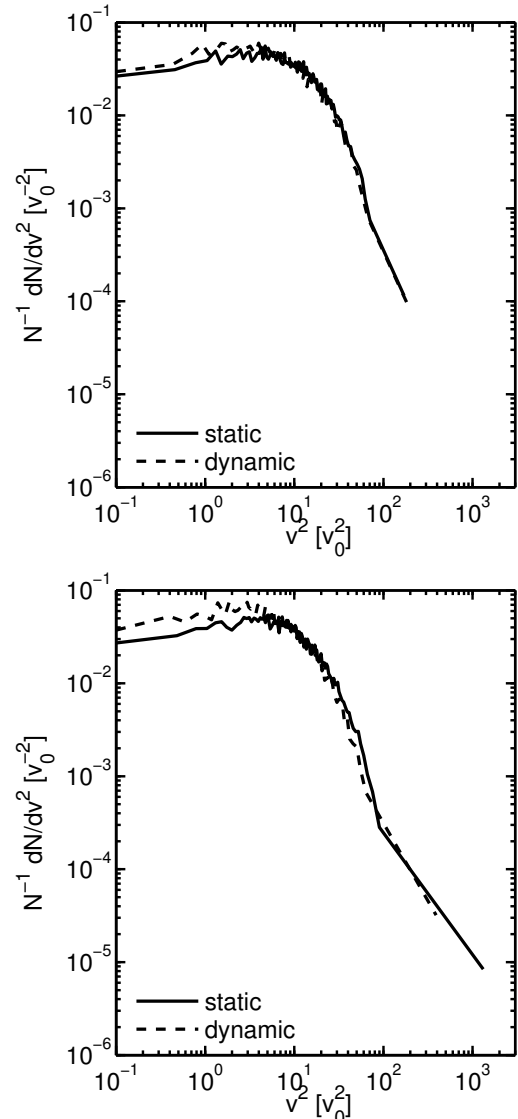


Figure 4. Probability density function of proton energies for the static and dynamic cases: (*Top*) Simulation without mean magnetic field ($B_0 = 0$) and (*Bottom*) simulation with mean magnetic field ($B_0 = 2$).

ing the guide field from zero up to a strong case with $B_0 = 8$.

3.2. Effect of B_0

The aim of this section is to show the effect of the mean magnetic field B_0 on the flow features, and on the resulting particle acceleration. It is well known that MHD flows with an imposed strong magnetic field suffer a transition from a three-dimensional (3D) state towards a two-dimensional (2D) state ([Alexakis \(2011\)](#); [Sujovolsky and Mininni \(2016\)](#)). The relevance of this anisotropy has been discussed by many authors in the recent years, specially in the context of the solar wind

Table 2. Parameters of the simulations with varying B_0 , discussed in Sec. III.B. B_0 is the amplitude of the guide field, $\langle v^2 \rangle$ and $\langle b^2 \rangle$ are respectively the mean kinetic and magnetic energies in the turbulent steady state (for a fluid with mass density $\rho = 1$), β is the plasma “beta,” $\langle L \rangle$ is the average energy containing scale for the flow during the steady-state period, $\langle k_d \rangle$ is the average Kolmogorov dissipation wavenumber, and α is the nominal particle gyroradius.

B_0	$\langle v^2 \rangle$	$\langle b^2 \rangle$	β	$\langle L \rangle$	$\langle k_d \rangle$	α
0	0.91	2.61	6.12	2.41	92	40
2	1.29	1.74	2.79	1.78	96	52.63
4	1.12	1.28	0.93	2.28	86	40
8	1.22	1.13	0.24	2.28	92.3	43.48

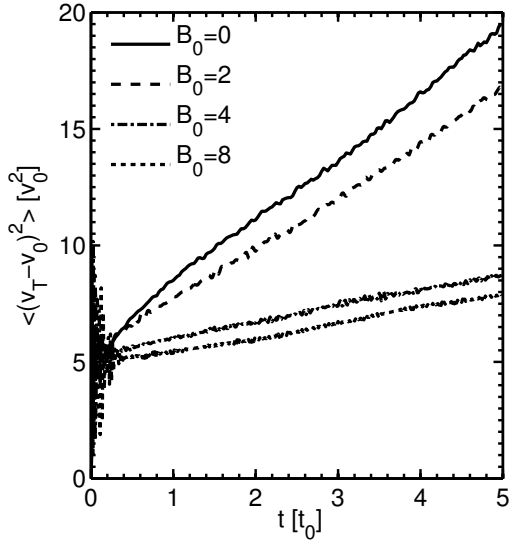


Figure 5. Mean square total velocity of protons as a function of time for different simulations, changing the mean magnetic field value B_0 .

problem. This transition from a 3D to a 2D state is accompanied by the transfer of energy towards modes with small parallel wavenumber (i.e., by the increase of the correlation length of the structures in the direction of the mean field Alexakis (2011)), and is associated with the development of the conditions that would establish an inverse cascade of the squared vector potential if the flow becomes 2D (Mininni et al. (2005); Wareing and Hollerbach (2010)). Both effects (although in different ways) result in the growth in size of the structures in the flow. We thus now look for the effect of the resulting anisotropic field and increased correlation lengths on test particle acceleration. In Table 2. we show the parameters of the simulations presented in this section. In the Table it can be noted that the plasma beta is

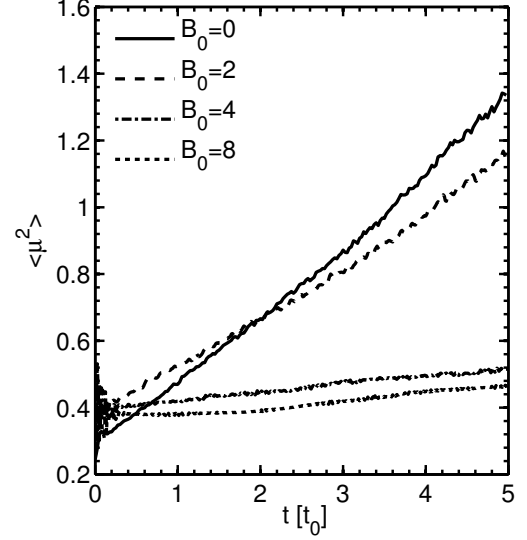


Figure 6. Mean square magnetic moment of protons as a function of time for different simulations, changing the mean magnetic field value B_0 .

not equal to 1 specially for the isotropic case. It is important to remark that the proton gyroradius and the proton inertial length are not rigorously equal in those simulations.

In Figure. 5 we show the r.m.s velocity as a function of time for all the simulations with different values of the mean magnetic field. It is observed that as the mean field increases, the particles velocity at the end of the simulation is reduced, and the acceleration process is thus diminished. The reduction of the r.m.s velocity with increasing mean magnetic field is an effect of the growth in the size of the structures; as current sheets become elongated (in the direction of the mean field resulting from the anisotropy), and wider (in the direction perpendicular to the mean field resulting from the flow two-dimensionalization), the particles get trapped in the structures (i.e. the particles are magnetized) and cannot easily be exposed for longer times to the accelerating gradient electric fields in the vicinity of current sheets.

As observed before, in the isotropic case ($B_0 = 0$) particles find structures distributed in all directions, and thus the final velocity is greater than in all the other cases with non-zero mean magnetic field. This is because the perpendicular energy gained by the the particle is decreased more substantially in presence of a strong mean magnetic field, confirming the argument about the effect of the anisotropy mentioned above.

In Figure. 6 we show the mean square magnetic moment for protons as funtion of time for all the simulations with different values of the mean magentic field. The magnetic moment $\mu = W_{\perp}/2B$, with W_{\perp} the perpen-

dicular energy of the particle, is one of the adiabatic invariant of charged particles dynamic in magnetic fields. It has important consequences in the dynamic of particles and determine how magnetized is a particle, that is how much attached is a particle to a magnetic field line. Variation of magnetic moment changes with turbulence parameters was studied in some detail by [Dalena et al. \(2012\)](#). It is observed that the mean square magnetic moment of protons increase its variation in time as the mean magnetic field is decreased. This means that protons become more demagnetized for lower values of the mean magnetic field. On the other hand, as the mean magnetic field is increased it can be observed an onset of magnetic moment conservation. This means that particles become magnetized (attached to the field lines). Then, in those cases, particles propagate along the mean field direction and the perpendicular crossing through different current sheet structures become suppressed.

The PDFs of the values of the electric field also help to understand this scenario. The PDFs of the electric field Cartesian components are shown in Figure. 7. The parallel (z component) of the electric field takes larger values in the isotropic case than in the anisotropic cases. As already mentioned, this is because current sheets in the former case are oriented in all directions, and the electric field is larger due to the large values of the velocity field. As B_0 is increased, the the parallel (z) electric field becomes weaker. The perpendicular (x component) of the electric field shows the opposite behavior: electric field values are larger as the mean magnetic field increases. This is caused mainly by the first term in equation. (10) (the term containing the mean magnetic field value). In spite of this, particle energization does not follow the same tendency because as noticed the particles cannot leave the currents structures and then cannot interact with strong electric field gradients in regions nearby the current sheets interfaces. That is, what is relevant for perpendicular particle energization is not the absolute value of the electric field but rather the exposure time of particles to strong gradients of that electric field.

To confirm this scenario, in Figure. 8 we show the x - y cross-section of the perpendicular component of the electric field E_x , and the x - z cross-section of E_x for all the simulations discussed in this section (from left to right we show the cases with $B_0 = 0$ up to the strongest case with $B_0 = 8$). The trajectory of three of the most energetic particles are shown as well with solid lines and marks (using plus, circles and crosses for each particle).

Note the particle behavior and the importance of the structure size on particle energization. In the isotropic case it is observed that the structures are distributed

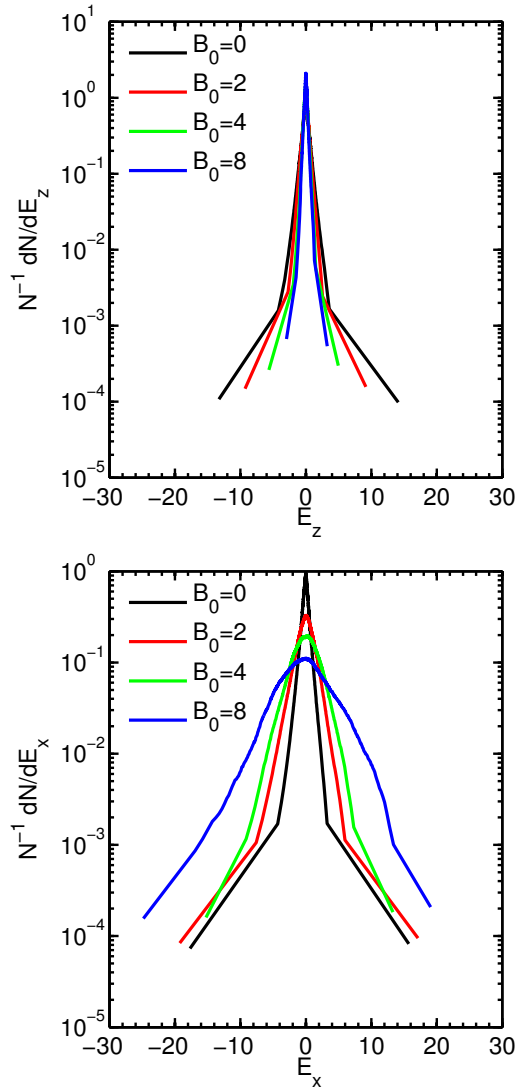


Figure 7. Probability distribution function of the electric field in all simulations. (*Top*) The parallel (z component) of the electric field E_z and (*Bottom*) The perpendicular (x component) of the electric field E_x .

in all directions, and there are no differences between both cross-sections of the electric field. In contrast, the cases with nonzero mean magnetic field show the structures aligned with the mean field as clearly seen in the bottom panels of Figure. 8. As the mean magnetic field increases, the flow becomes more anisotropic and for the strongest mean field the variations in the z direction are small.

The x - y cross-sections give us an idea of the size of the structures. It is observed that as the mean magnetic field increases, the width of the structures also increase, and a transition from a flow with randomly distributed structures with a width of the order of the dissipation

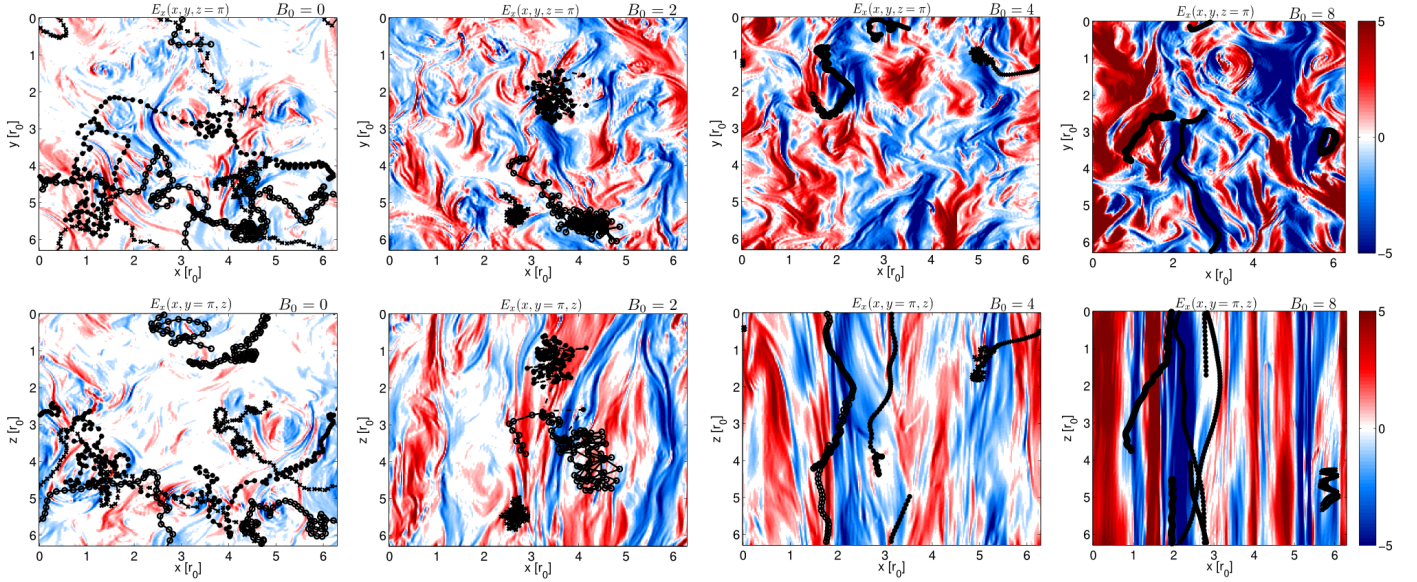


Figure 8. (Top row) x - y cross-section of the perpendicular (x component) electric field (E_x) in the simulation box, for different values of B_0 . (Bottom row) x - z cross-section of the perpendicular (x component) electric field (E_x). In both rows, from left to right, the following simulations are shown: $B_0 = 0$, $B_0 = 2$, $B_0 = 4$, and $B_0 = 8$ respectively. The black signs and lines show the trajectories of three of the most energetic protons in each simulation.

scale can be seen for the isotropic case, moving towards a flow with wider structures in the cases with a non-zero mean magnetic field.

The trajectories of the particles show the importance of the structure size. While trajectories reminiscent of stochastic motion are observed at the isotropic case, where the particle passes through many structures finding strong electric field gradient regions along its path, as the mean magnetic field increases the particle trajectories become more elongated and particles cannot go across structures. For the $B_0 = 4$ and $B_0 = 8$ cases, the trajectories show that particles drift across a few structures, almost staying around a single one and no longer allowing the particle to stay in strong electric field gradient regions. This is the reason why particles do not gain as much energy as in the isotropic case, as the random hopping from one structure to the next is the most efficient acceleration mechanism as observed in [Gonzalez et al. \(2016\)](#).

4. DISCUSSION:

In this paper we studied the effect of dynamically evolving MHD turbulence on test particle acceleration. To this end, we solved numerically the MHD equations, and solved the equations for test particles either together with the flow evolution, or in frozen-in-time fields obtained from snapshots of the electromagnetic fields in the MHD simulations. This case of “static MHD turbulence” has been used before to investigate particle energization phenomena ([Dmitruk et al. \(2004\)](#); [Dalena et al.](#)

(2014); [Gonzalez et al. \(2016\)](#)). We found some differences between both models, with a slight reduction of particle acceleration in the dynamical case. This result was obtained for “protons,” or test particles with gyro-radius of the order of the flow dissipation scale, which is the case we specifically analyzed here. The reduction in the acceleration rate is due to particle trapping in the dynamic current structures, that makes more difficult for particles to move through strong electric field gradient regions located at the interface between structures whereby particles are accelerated.

The study was motivated by the fact that several of the previous works done on particle acceleration considered static MHD turbulence. Even though there are some previous papers which have deal with dynamic problem([Cho and Lazarian \(2006\)](#); [Weidl et al. \(2015\)](#); [Teaca et al. \(2014\)](#); [Hussein and Shalchi \(2016\)](#)), most of those studies consider incompressible flow models. Also, a detailed comparison between static and dynamic fields and their effect of particle acceleration was lacking.

This paper is most closely related with [Lehe et al. \(2009\)](#) due to the compressible turbulence and dynamic model which both have used. In that paper the authors conclude that the particle heating is due to the cyclotron resonance with Alfvén waves in the system when the waves frequencies are of the order of the particle gyrofrequency. In this paper we have shown that the perpendicular proton heating is almost the same for the dynamic and static cases, which means that we can obtain the same results with or without allowing waves

in the system. In fact, this result is very important because it confirms the importance of coherent structures in particle energization. Also, the authors discussed about the relevance of the results in the context of solar wind and solar corona, and they claim that the results can not be directly applied to those astrophysical systems, mainly because the limitation of numerical resolution and the short scale separation one can obtain using this numerical method. We agree with the authors about the need to extrapolate these results to a higher numerical resolution which would lead to recreate closely the corona and solar wind.

Additionally, we investigated the effect of anisotropy caused by the mean magnetic field on the resulting particle acceleration, for which it was observed an important adverse effect on particle energization. The transition from a three-dimensional towards a two-dimensional MHD state, which can be also accompanied by an inverse energy cascade for very strong magnetic guide fields, causes an increase in the structure sizes, impacting on the reduction of the particle acceleration as test particles are trapped in wider current channels, and exhibit an almost magnetized state with, in average, conservation of magnetic moment.

Considering the results reported in Gonzalez et al. (2016), where we showed that the flow compressibility affects particle energization, in this work we made sure that no important variations in the turbulent Mach number were present between different runs. To this end we also considered forced simulations (instead of freely decaying ones), to be able to study particle acceleration in a turbulent steady state with a well defined mean Mach number. To prevent effects associated with a possible inverse cascade of magnetic helicity, or of cross-correlations between the velocity and magnetic fields, we implemented a forcing mechanism that warrants no net injection of kinetic helicity, magnetic helicity, or cross-helicity.

In the same way, the model we use in this paper for the test particles includes electron pressure effects and

the Hall current in the generalized Ohm's law for particle motion computation. It is noted that we have not included those terms in the induction equation based on the assumption that we can neglect them at large fluid scales Dmitruk and Matthaeus (2006). While retaining those effects for particle motion we found that pressure effects can have an important contribution to the energization of particles with small gyroradius Gonzalez et al. (2016) (compared with the width of the current sheets). For particles with gyroradius of the order of the MHD dissipation scale (called "protons" here) these effects are not important, with the main mechanism responsible for acceleration being the MHD electric field and its fast changes as the particles move from one current sheet to another, allowing particles to be exposed to strong electric field gradients at the interface of the structures.

The results support and reaffirm the importance of coherent structures on particle acceleration, and their possible relevance for the solar wind. This latter problem has been analyzed using different approaches, from spacecrafts data measurements (Tessein et al. (2015)) to different numerical schemes covering fluid and kinetic descriptions (Ambrosiano et al. (1988); Greco et al. (2008); Servidio et al. (2014); Karimabadi et al. (2013); Drake et al. (2006)). The coherent structures in this case appear by the interaction and pileup of magnetic flux tubes, and those regions provide the possibility of generating strong field gradients, where particles can experience substantial energization.

C.A.G., P.D.M., and P.D. acknowledge support from grants UBACyT No. 20020110200359 and 20020100100315, and from grants PICT No. 2011-1529 and 2011-0454. W.H.M. was partially supported by NASA LWS-TRT grant NNX15AB88G, Grand Challenge Research grant NNX14AI63G, and the Solar Probe Plus mission through the Southwest Research Institute ISIS project D99031L.

REFERENCES

- Alexandros Alexakis. Two-dimensional behavior of three-dimensional magnetohydrodynamic flow with a strong guiding field. *Phys. Rev. E*, 84:056330, Nov 2011. doi:10.1103/PhysRevE.84.056330. URL <http://link.aps.org/doi/10.1103/PhysRevE.84.056330>.
- John Ambrosiano, William H. Matthaeus, Melvyn L. Goldstein, and Daniel Plante. Test particle acceleration in turbulent reconnecting magnetic fields. *Journal of Geophysical Research: Space Physics*, 93(A12): 14383–14400, 1988. ISSN 2156-2202. doi:10.1029/JA093iA12p14383. URL <http://dx.doi.org/10.1029/JA093iA12p14383>.

- Benjamin D. G. Chandran. *The Astrophysical Journal*, 599 (2):1426, 2003. URL <http://stacks.iop.org/0004-637X/599/i=2/a=1426>.
- Benjamin D. G. Chandran and Jason L. Maron. *The Astrophysical Journal*, 603(1):23, 2004. URL <http://stacks.iop.org/0004-637X/603/i=1/a=23>.
- Jungyeon Cho and A. Lazarian. *The Astrophysical Journal*, 638(2):811, 2006. URL <http://stacks.iop.org/0004-637X/638/i=2/a=811>.
- S. Dalena, A. Greco, A. F. Rappazzo, R. L. Mace, and W. H. Matthaeus. Magnetic moment nonconservation in magnetohydrodynamic turbulence models. *Phys. Rev. E*, 86:016402, Jul 2012. doi:10.1103/PhysRevE.86.016402. URL <https://link.aps.org/doi/10.1103/PhysRevE.86.016402>.
- S. Dalena, A. F. Rappazzo, P. Dmitruk, A. Greco, and W. H. Matthaeus. *The Astrophysical Journal*, 783(2): 143, 2014. URL <http://stacks.iop.org/0004-637X/783/i=2/a=143>.
- P. Dmitruk and W. H. Matthaeus. Test particle acceleration in three-dimensional hall mhd turbulence. *Journal of Geophysical Research: Space Physics*, 111 (A12):n/a–n/a, 2006. ISSN 2156-2202. doi:10.1029/2006JA011988. URL <http://dx.doi.org/10.1029/2006JA011988>. A12110.
- Pablo Dmitruk, W. H. Matthaeus, and N. Seenu. *The Astrophysical Journal*, 617(1):667, 2004. URL <http://stacks.iop.org/0004-637X/617/i=1/a=667>.
- J. F. Drake, M. Swisdak, H. Che, and M. A. Shay. Electron acceleration from contracting magnetic islands during reconnection. *Nature*, 443(7111):553–556, October 2006. ISSN 0028-0836. URL <http://dx.doi.org/10.1038/nature05116>.
- C. A. Gonzalez, P. Dmitruk, P. D. Mininni, and W. H. Matthaeus. On the compressibility effect in test particle acceleration by magnetohydrodynamic turbulence. *Physics of Plasmas*, 23(8):082305, 2016. doi:http://dx.doi.org/10.1063/1.4960681. URL <http://scitation.aip.org/content/aip/journal/pop/23/8/10.1063/1.4960681>.
- A. Greco, P. Chuychai, W. H. Matthaeus, S. Servidio, and P. Dmitruk. Intermittent mhd structures and classical discontinuities. *Geophysical Research Letters*, 35(19): n/a–n/a, 2008. ISSN 1944-8007. doi:10.1029/2008GL035454. URL <http://dx.doi.org/10.1029/2008GL035454>. L19111.
- M. Hussein and A. Shalchi. Simulations of energetic particles interacting with dynamical magnetic turbulence. *The Astrophysical Journal*, 817(2):136, 2016. URL <http://stacks.iop.org/0004-637X/817/i=2/a=136>.
- H. Karimabadi, V. Roytershteyn, M. Wan, W. H. Matthaeus, W. Daughton, P. Wu, M. Shay, B. Loring, J. Borovsky, E. Leonardis, S. C. Chapman, and T. K. M. Nakamura. Coherent structures, intermittent turbulence, and dissipation in high-temperature plasmas. *Physics of Plasmas*, 20(1):012303, January 2013. doi:10.1063/1.4773205.
- R.M. Kulsrud. *MHD description of plasma*, in *Basic Plasma Physics: Selected Chapter*. AA Galeev, RN Sudan, 1983.
- A. Lazarian, L. Vlahos, G. Kowal, H. Yan, A. Beresnyak, and E.M. de GouveiaDalPino. *Space Science Reviews*, 173(1-4):557–622, 2012. ISSN 0038-6308. doi:10.1007/s11214-012-9936-7. URL <http://dx.doi.org/10.1007/s11214-012-9936-7>.
- Rémi Lehe, Ian J Parrish, and Eliot Quataert. The heating of test particles in numerical simulations of alfvénic turbulence. *The Astrophysical Journal*, 707(1):404, 2009.
- Jacob W. Lynn, Eliot Quataert, Benjamin D. G. Chandran, and Ian J. Parrish. *The Astrophysical Journal*, 777(2): 128, 2013. URL <http://stacks.iop.org/0004-637X/777/i=2/a=128>.
- W. H. Matthaeus, J. J. Ambrosiano, and M. L. Goldstein. *Phys. Rev. Lett.*, 53:1449–1452, Oct 1984. doi:10.1103/PhysRevLett.53.1449. URL <http://link.aps.org/doi/10.1103/PhysRevLett.53.1449>.
- D. J. McComas, M. Velli, W. S. Lewis, L. W. Acton, M. Balat-Pichelin, V. Bothmer, R. B. Dirling, W. C. Feldman, G. Gloeckler, S. R. Habbal, D. M. Hassler, I. Mann, W. H. Matthaeus, R. L. McNutt, R. A. Mewaldt, N. Murphy, L. Ofman, E. C. Sittler, C. W. Smith, and T. H. Zurbuchen. Understanding coronal heating and solar wind acceleration: Case for in situ near-sun measurements. *Reviews of Geophysics*, 45(1): n/a–n/a, 2007. ISSN 1944-9208. doi:10.1029/2006RG000195. URL <http://dx.doi.org/10.1029/2006RG000195>. RG1004.
- Pablo D Mininni. Scale interactions in magnetohydrodynamic turbulence. *Annual Review of Fluid Mechanics*, 43:377–397, 2011.
- Pablo D Mininni, David C Montgomery, and Annick G Pouquet. A numerical study of the alpha model for two-dimensional magnetohydrodynamic turbulent flows. *Physics of Fluids (1994-present)*, 17(3):035112, 2005.

- Pablo D. Mininni, Duane Rosenberg, Raghu Reddy, and Annick Pouquet. A hybrid mpiopenmp scheme for scalable parallel pseudospectral computations for fluid turbulence. *Parallel Computing*, 37(67):316 – 326, 2011. ISSN 0167-8191. doi:<http://dx.doi.org/10.1016/j.parco.2011.05.004>. URL <http://www.sciencedirect.com/science/article/pii/S0167819111000512>.
- E. N. Parker and D. A. Tidman. Suprathermal particles. *Phys. Rev.*, 111:1206–1211, Sep 1958. doi:10.1103/PhysRev.111.1206. URL <http://link.aps.org/doi/10.1103/PhysRev.111.1206>.
- A. Pouquet and G. S. Patterson. Numerical simulation of helical magnetohydrodynamic turbulence. *Journal of Fluid Mechanics*, 85(2):305–323, 03 1978. doi:10.1017/S0022112078000658.
- S. Servidio, K. T. Osman, F. Valentini, D. Perrone, F. Califano, S. Chapman, W. H. Matthaeus, and P. Veltri. Proton kinetic effects in vlasov and solar wind turbulence. *The Astrophysical Journal Letters*, 781(2): L27, 2014. URL <http://stacks.iop.org/2041-8205/781/i=2/a=L27>.
- N. E. Sujovolsky and P. D. Mininni. Tridimensional to bidimensional transition in magnetohydrodynamic turbulence with a guide field and kinetic helicity injection. *Phys. Rev. Fluids*, 1:054407, Sep 2016. doi:10.1103/PhysRevFluids.1.054407. URL <http://link.aps.org/doi/10.1103/PhysRevFluids.1.054407>.
- Bogdan Teaca, Martin S. Weidl, Frank Jenko, and Reinhard Schlickeiser. *Phys. Rev. E*, 90:021101, Aug 2014. doi:10.1103/PhysRevE.90.021101. URL <http://link.aps.org/doi/10.1103/PhysRevE.90.021101>.
- Jeffrey A. Tessein, David Ruffolo, William H. Matthaeus, Minping Wan, Joe Giacalone, and Marcia Neugebauer. Effect of coherent structures on energetic particle intensity in the solar wind at 1 au. *The Astrophysical Journal*, 812(1):68, 2015. URL <http://stacks.iop.org/0004-637X/812/i=1/a=68>.
- Christopher J. Wareing and Rainer Hollerbach. Cascades in decaying three-dimensional electron magnetohydrodynamic turbulence. *Journal of Plasma Physics*, 76(1):117–128, 002 2010. doi:10.1017/S0022377809990158.
- Martin S. Weidl, Frank Jenko, Bogdan Teaca, and Reinhard Schlickeiser. *The Astrophysical Journal*, 811(1):8, 2015. URL <http://stacks.iop.org/0004-637X/811/i=1/a=8>.